Desalination and Water Treatment
www.deswater.com
doi: 10.1080/19443994.2013.822165

52 (2014) 6802–6816
October

Taylor & Francis
Taylor & Francis Group

Integrated synthesis and characterization of some porous polyacrylamide-based composites for cationic sorption from aqueous liquid wastes

I.M. El-Naggar[a], G.M. Ibrahim[a,b], B. EL-Gammal[a,*], E.A. El-Kady[a]

[a]*Hot Laboratories Center, Atomic Energy Authority, P. No. 13759, Cairo, Egypt*
Email: belalelgammal@hotmail.com
[b]*King Khaled University, Bisha Branch, Bisha, Kingdom of Saudi Arabia*

Received 12 February 2012; Accepted 16 June 2013

ABSTRACT

Three types of polymeric–inorganic composite cation-exchangers were synthesized by impregnation of inorganic precipitates of tin(IV) silicate and tin(IV) antimonate with different ratios into polyacrylamide matrices to form polyacrylamide stannic silicate (PAmSnSi), polyacrylamide stannic antimonate (PAmSnSb), and polyacrylamide stannic silicoantimonate (PAmSnSiSb) hybrid composites. These materials were characterized by X-ray powder diffraction, FTIR, SEM, BET surface area, DTA, and TGA. They possessed high surface areas with mesoporous texture; PAmSnSi, PAmSnSb, and PAmSnSiSb exhibited type IV-H4, IV-H3, and IV-H2 N_2-adsorption, respectively. They showed improved chemical stabilities which was in the order of PAmSnSb > PAmSnSi > PAmSnSiSb in HNO_3, while their stability order in HCl was PAmSnSi > PAmSnSb > PAmSnSiSb. The effect of experimental parameters such as temperature, concentration, and pH on the properties of material has been studied. Distribution behaviors for radioactive aqueous $^{134}Cs^{+}$, $^{60}Co^{2+}$, and $^{90}Sr^{2+}$ as well as Cd^{2+} ions on the three composite ion exchangers were investigated to understand the cation-exchange performance of the materials; some binary separations were predicted and compared.

Keywords: Porous materials; Synthesis; Characterization; Sorption and radioactive waste

1. Introduction

New technology development for air and water purification is of importance due to the increasing concerns of both growing national security and human health [1,2]. Specifically, the radionuclides and toxic metal ions present in water are injurious to the health. Hence, it is very important to treat such water by removal of these hazardous ions before it is supplied for any useful purpose [1–4]. The optimization of wastewater purification processes requires a development of new operations based on low-cost raw materials with high-pollutant removal efficiency [5,6]. A number of different techniques has studied removal of the radionuclides from the waste effluents. Ion exchange is considered to be of effective separation technique with acceptable results [7,8]. The ion exchangers are termed to contain ions that are exchangeable with others existing in a solution in which it is considered to be insoluble. Various types of inorganic and organic ion exchangers have been synthesized; however, inorganic ion exchangers generally are superior to organic resins because of their greater

*Corresponding author.

resistance at high temperature and high radiation, which is of great importance in the nuclear technology [9–11]. Moreover, they have unusual selectivity for ionic species and versatility in separation sciences.

Although the organic ion exchangers have a wide applicability, but a few limitations of the organic resins have been reported. One of the major limitations of the organic resins is their poor thermal stability. Since organic ion exchangers were found to be unstable at high temperature and strong radiation, inorganic ion exchangers were taken as alternatives. However, the inorganic ion exchangers also have their own limitations, for example, unsuitable for column operation because of nongranulomatotic nature. In order to overcome the above limitations of both organic resins and inorganic ion exchangers, many investigators have introduced organic–inorganic composite ion exchangers consisting of inorganic materials and organic binding matrices [12–14]. In literature, various methods of preparing these crossbred materials have been reported [15–17]. Composite materials formed by mixing organic polymers and inorganic salts possess all the good properties of both the constituents and an enhanced utility. The combination of organic and inorganic precursors yields hybrid materials that have mechanical properties not present in the pure materials. The organic group can be reactive, which implies that it can form an organic network as well as inorganic network. In designing composite materials, scientists, and engineers have ingeniously combined various metals, ceramics, and polymers to produce a latest generation of extraordinary materials that encompass a wide variety of applications [18–20]. Most composites have been created to improve combination of mechanical characteristics such as stiffness, toughness, and high temperature strength. Thus, the synthesis of polymeric–inorganic composite has received a great deal of attention because it provided modern material with special mechanical, chemical, electrochemical, and optical as well as magnetic properties [21,22].

The following study summarizes the preparation, characterization, and analytical applications of newly synthesized hybrid cation exchanger, PAmSnSi, PAmSnSb, and PAmSnSiSb. Separation of $^{134}Cs^{+}$, $^{60}Co^{2+}$, $^{90}Sr^{2+}$, and Cd^{2+} metal ions have been studied in light of distribution coefficients.

2. Materials and methods

2.1. Chemicals and reagents

All the reagents used were of analytical grade and used without further purification. In all experiments, demineralized water (DMW), was used for preparation, dilution and for final washing of the sorbent. Sodium silicate was supplied by Sigma-Aldrich with a typical chemical formula, Na_2O_3Si; molar mass, 122.06 g/mol and is considered as three H-bond acceptor. However, it has ignition temperature, 424°C; Solubility in water, 2040 g/l (25°C); Melting point, 84°C.

Antimony pentacholride with hill formula Cl_5Sb; chemical formula $SbCl_5$; molar mass 299.01 g/mol; solubility (20°C) (rigorous decomposition); melting point 3–4°C; molar mass 299.01 g/mol; density 2.35 g/cm^3 (20°C); boiling point 140°C; vapor pressure 1.1 hPa (20°C) was supplied by Merck chemicals, Darmstadt, Germany.

Acrylamide monomer, supplied by Sigma-Aldrich, USA Hill Formula C_3H_5NO; chemical formula $CH_2CHCONH_2$; molar mass 71.07 g/mol; ignition temperature 424°C; solubility 2040 g/l (25°C); melting point 84°C; molar mass 71.07 g/mol; density 1.127 g/cm^3 (25°C); bulk density 500 kg/m^3; pH value 5.0–7.0 (50 g/l, H_2O, 20°C); boiling point 125°C (33.3 hPa) and vapor pressure 0.009 hPa (20°C) was used as a base monomer for polyacrylamide preparation.

2.2. Synthesis of composite ion exchangers

Poly acryl amide (PAm) was prepared by adding 2% PAm in 200 ml DMW with continuous stirring for 2 h until a white gel was obtained, using potassium persulfate as an initiator at 70 ± 5°C. After that the gel was transferred into the pale white precipitate of inorganic ion exchanger Sn(IV)antimonate, which is prepared by adding one volume of 1 M tin solution prepared in 100 ml aqua regia, then added to two volumes of antimony chloride, mixed thoroughly with constant stirring. These slurries were refluxed for 2 h at a temperature of 70 ± 1°C. The resultant products were left for 24 h at room temperature for digestion. At the final stage, the composite cation-exchanger gels were filtered off; washed with DMW to remove excess acid. The washed gel dried at 40°C, cracked into small granules and converted into to Na^{+}-form by treating with 0.05 M NaOH for 24 h with occasional shaking intermittently replacing the supernatant liquid with fresh base. The excess base was removed after several washings with DMW and finally dried at 50°C and sieved to obtain different particle sizes.

Polyacrylamide tin(IV) silicate, PAmSnSi was prepared by adding one volume of 1.2 M tin solution prepared in 100 ml aqua regia, then added to five volumes of sodium silicate. The white precipitates were obtained, when the pH of the mixtures was adjusted 8.4 adding aqueous ammonia with firm stirring. The gels of polyacrylamide were added into the white

inorganic precipitate of Sn (IV) silicate mixed thoroughly with continuous stirring. These slurries were refluxed for 2 h at a temperature of 70 ± 1 ℃ and were kept for 24 h at room temperature (25 ± 2 ℃). The materials were dried in an air oven 50 ℃. The dried products were immersed in DMW to obtain small granules. They were converted to Na^+-form by treating with 0.05 M NaOH for 24 h with occasional shaking intermittently replacing the supernatant liquid with fresh base. The excess base was removed after several washings with DMW, and finally dried at 50 ℃ and sieved to obtain different particles size and kept in desiccators.

The organic–inorganic composite cation exchanger, polyacrylamide tin (IV) silicoantimonate (PAmSnSiSb) was prepared by the same procedures described for polyacrylamide stannic silicate (PAmSnSi) and polyacrylamide stannic antimonate (PAmSnSb), by adjusting PAmSnSi and PAmSnSb to be 1:1 M ratio at 70 ± 1 ℃. Ammonia solution was then added to hydrolyze the above solution. A pale yellow precipitate was obtained, which was washed with DMW after overnight standing for several times, until the pH of the supernatant solution maintain constant at eight. The obtained product was treated with 0.05 M NaOH solution for 24 h, then washed with DMW, dried at 50 ± 1 ℃ and sieved to obtain different mesh sizes.

2.3. Chemical stability

The chemical stability of the composite ion exchanger was tested in H_2O, HCl, and HNO_3 in various concentrations was tested. Hundred milligram of the sorbent was equilibrated with 50 ml of the aqueous solution with intermittent shaking for 48 h. The filtrate was tested for calculation of the percent of solubility of the PAmSnSi in different media.

2.4. Thermal stability

One gram of the material was heated to various temperatures (50, 100, 200, 400, and 600 ℃); the thermal stabilities of the materials were augmented by measuring the water content of the prepared sorbents as a function of temperature.

2.5. Characterization

Powder X-ray diffraction was performed using the Shimadzu X-ray diffractometer (XRD), model XD610 (Japan), with a nickel filter, and CuKα radiation at 1.54 Å, operating at 30 kV and 30 mA.

The FTIR spectra were acquired with a Bomem FTIR model MB 157 produced from Canada. Applying KBr disc technique where a compress KBr pellets containing 6% sample were used to this purpose. The wave number range was from 4,000–400 cm^{-1} with resolution 4 cm^{-1} and wave number accuracy 1 cm^{-1}.

The texture of cement/bitumen samples was observed with SEM by JEOL-JSM5-5400, Japan, which enables magnification to 50X.

The thermal behavior of the prepared exchangers and samples was carried out using Shimadzu simultaneous DTA and TGA-60H caloric analyzer obtained from a Shimadzu Kyoto, Japan. The samples measured from ambient temperature up to 600 ℃ with a heating rate of 10 ˚/min under a nitrogen atmosphere.

2.6. Batch distribution studies

The distribution coefficients were carried out in batch mode by mixing 40 mg of 10^{-4} M of each of $^{134}Cs^+$, $^{60}Co^{2+}$, $^{90}Sr^{2+}$, and Cd^{2+} ions solutions for different pH values and unlike reaction temperatures (30, 45 and 60 ℃); samples were shaken in a shaker thermostatic at 30 ℃ for 24 h to attain equilibrium distribution for the system studied. Liquids were separated from the solids, the equilibrium pH was determined and the corresponding $^{134}Cs^+$, $^{60}Co^{2+}$, and $^{90}Sr^{2+}$ activity (Cd^{2+} ion concentration) were measured. The uptake of $^{134}Cs^+$, $^{60}Co^{2+}$, $^{90}Sr^{2+}$, and Cd^{2+} ion was then calculated, from which the distribution coefficient will be calculated according to the formula:

$$\% \text{ Uptake} = \frac{I_0 - I}{I_0} \times 100 \quad (1)$$

$$K_d = \frac{\% \text{ Uptake}}{100 - \% \text{ Uptake}} \times \frac{V}{m} \quad (2)$$

where I_0 is the initial activity (concentration in case of Cd^{2+} ions) of the solution, and I is the final activity (concentration) of the solution.

In all batch experiments, atomic absorption spectrophotometer (Buck Scientific) model VGP 210 using air acetylene flame, England was used to analyze the solution. However, the radioactive nuclides of ^{134}Cs, ^{60}Co, and ^{90}Sr used for this study were assayed by measuring their gamma-ray activities in both solid and solution phases using NaI (TI) scintillation detector connected to a scalar of SR7 type obtained from Enterprises, USA.

Table 1
Chemical stability of the composite ion exchangers PAmSnSi, PAmSnSb, and PAmSnSiSb at different acid concentration

Sample	Solubility %									
	H_2O	HNO_3 (M)					HCl (M)				
		0.1	0.5	1	2	4	0.1	0.5	1	2	4
SAM	BD	4	4.8	5.8	6	7.7	3.2	3.6	4.8	5	6.6
FAM	BD	3.4	3.6	5.2	5.44	5.82	4.8	5.6	5.8	8.2	10
NORAM	BD	3	7.6	8.8	12	15.4	6.2	12.4	12.6	13	15.2

BD: Below detection.

3. Results and discussion

3.1. Chemical stability

The chemical stability of the prepared PAmSnSi, PAmSnSb, and PAmSnSiSb was studied in DMW, HNO_3 and HCl at 0.1, 0.5, 1, 2, and 4 M, by mixing 100 mg of each of the prepared specimens and 100 ml of the testing solution with intermittent shaking for about one week at 25 ± 1 ℃. The filtrate was checked using ICP, while the solid content was gravimetrically investigated. The results are represented in Table 1. PAmSnSi, PAmSnSb, and PAmSnSiSb have good chemical stability; they can withstand the effect of acids to a great extent; they are resistant to 4 M HNO_3 and 4 M HCl. The solubility in the HNO_3 was higher than in the HCl. Furthermore, the results indicated that the chemical stability of PAmSnSb > PAmSnSi > PAmSnSiSb in HNO_3 while the chemical stability order in HCl is as follows: PAmSnSi > PAmSnSb > PAmSnSiSb.

The PAmSnSi, PAmSnSb, and PAmSnSiSb hybrid organic–inorganic ion exchangers are more stable than polyacrylamide Sn(IV) molybdophosphate and Sn(IV) molybdophosphate [23], polypyrrole/Fe_3O_4 nanocomposite [24], especially at high acid concentration (4 M HCl and 4 M HNO_3), also the prepared material has high chemical stability by comparison to cerium titanate, which has solubility % at 3 M HNO_3 and HCl as 16.21 and 17.18%, respectively [25]. While EGIB sorbent [26] are more stable than the prepared material for this study. This chemical stability may be due to the presence of binding polymer, which can prevent the dissolution of heteropolyacid salt or leaching of any constituent elements from the solution [27].

3.2. X-ray diffraction

The XRD studies indicated that PAmSnSi and PAmSnSb are completely amorphous, while PAmSnSiSb possessed a very low degree of crystallinity.

3.3. Thermal behaviors and stabilities

The differential thermal analyses of the PAmSnSi, PAmSnSb, and PAmSnSiSb composites are shown in Figs. 1–3. In PAmSnSi resin, the onset-offset TGA weight loss temperature was at about 80–500 ℃, which elucidate the stability of the composites at high temperatures. On the other hand, the DTA scan revealed that a broad endothermic band was observed at about 80–350 ℃; it was considered a compound one as multi-type water removal mechanisms [17,18]. The total weight loss order was in PAmSnSi, 18% < PAmSnSb, 30% < PAmSnSiSb, 75%. These behaviors could be explained by the beginning of degradation of organic content at about 300 ℃, as indicated by the exothermic peaks at about 300 ℃ (Figs. 2 and 3). Other endothermic peaks were observed at about 358 and 339 ℃, due to movement of the organic chains as an effect of heat changes [21,22]. A complete burning of the organic polymer would be expected after 500 ℃ [21].

3.4. Surface characteristics

In Fig. 4, three different types of N_2 adsorption–desorption isotherms as observed for porous organic–inorganic resins are plotted. PAmSnSi, PAmSnSb, and PAmSnSiSb may be classified as a type IV-H4, IV-H3, and IV-H2 isotherms.

In PAmSnSb (H3) and PAmSnSi (H4) hysteresis, sloping adsorption and desorption branches covers a wide range of P/P_o with slit-like-pores with slightly out pores in case of H3 [28].

On the other hand, In PAmSnSiSb, H2, hysteresis equilibration takes longer if diffusion is limited due to blocking of the pore window by pore liquid, as represented by the critical loading of liquids. The descending branch from the loop shows a pronounced *plateau* followed by a steep fall. This behavior agrees with experimental isotherms of powder compacts compressed at gradually elevated pressures. When the

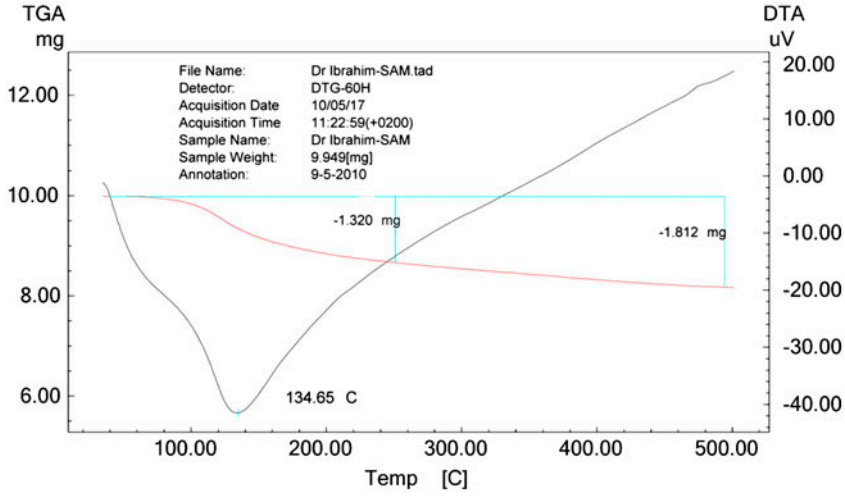

Fig. 1. DTA-TGA curves for PAmSnSi ion exchanger.

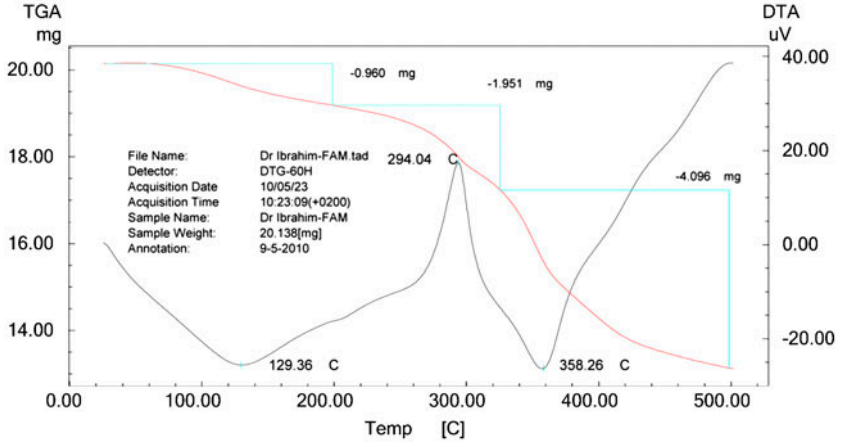

Fig. 2. DTA-TGA curves for PAmSnSb ion exchanger.

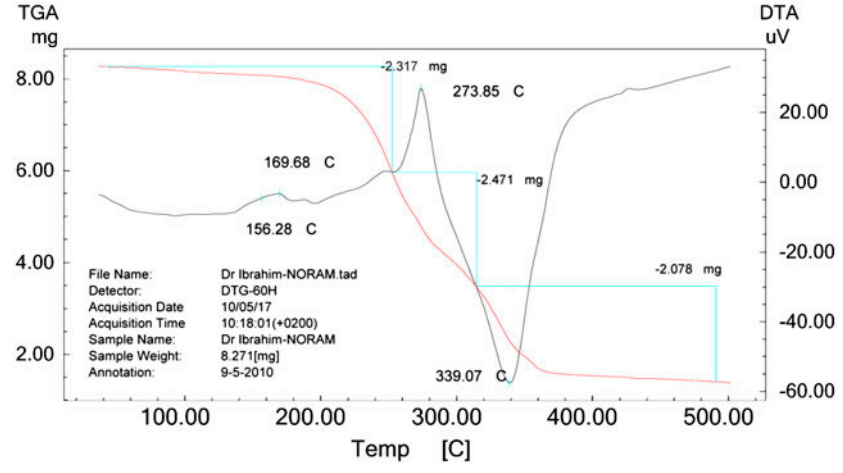

Fig. 3. DTA-TGA curves for PAmSnSiSb ion exchanger.

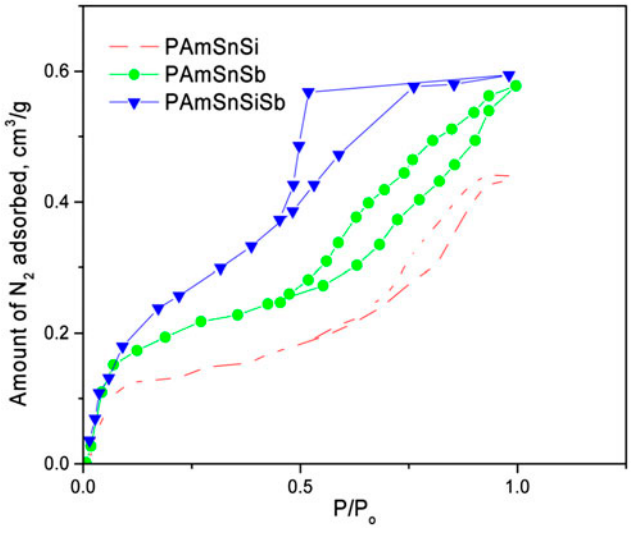

Fig. 4. N_2 adsorption–desorption isotherms measured on porous PAmSnSi, PAmSnSb, and PAmSnSiSb.

powder is uncompressed, it shows an isotherm of type II with no hysteresis. As compaction increases, a hysteresis loop of type H1 develops, and then evolves into the type H2. Meanwhile, the type II shape of the isotherm evolves into a type IV. The extent of uptake at the saturation vapor pressure becomes lower. In an overview, the type H2 behavior may be described according to the following mechanism [29].

(1) The ascending path deviates further from the true isotherm at the onset of the critical uptake, where diffusion becomes seriously limited.
(2) Since adsorption takes place minimally, the uptake never reaches the possible maximum at the saturation vapor pressure. Desorption delayed until the path crosses the true equilibrium, starts very slowly at the beginning because of the limited diffusion.
(3) As the uptake reaches the critical loading, the trapped (supersaturated) pore liquid diffuses away quickly to equilibrate with the bulk gas.

This behavior agrees with the pore-blocking theory by Everett in that evaporation from the pore is assumed to delay until the pore neck is cleared. However, the pore-blocking theory assumes complete filling of pores across the pore neck along the course of adsorption. Lack of the transport barrier in the pore-filling process is the major difference from the present theory [30].

From the experimental isotherms, the average pore size was calculated using **B**arrett, **J**oyner and **H**alenda, **BJH** equation. It was assumed that the pores are cylindrical, and all have the same length, the internal surface area of a single pore will be proportional to the radius of the pore (i.e. the pore size). Thus, the data would indicate that each of the measured samples has roughly the same number of pores; the differences in surface area per volume of porous material simply come from the difference in pore size. The average mesopore width determined from the BJH equation, D_{AV}^{BJH} is in the order of PAmSnSi (15.98 ± 0.06 nm) > PAmSnSb (12.37 ± 0.03 nm) > PAmSnSiSb (8.65 ± 0.04 nm). On the other side, the recorded specific surface area using BET method was in a reverse order, that is, S_{BET} for PAmSnSi, PAmSnSb, and PAmSnSiSb are about 145.56 ± 0.25, 189.72 ± 0.34, 326.80 ± 0.91 m^2/g. These values agree with the specific surface area by α-*s* method, Sα as, 147.84 ± 0.233, 190.67 ± 0.344, 328.78 ± 0.911 m^2/g. On the other hand, the total pore volume, V_t^p of the prepared composites are slightly lower that some activated carbon xerogels (2 order of magnitude) and recorded V_t^p values as 0.41 ± 0.02, 0.56 ± 0.02, and 0.59 ± 0.04 cm^3/g, for PAmSnSi, PAmSnSb, and PAmSnSiSb, respectively [31].

3.5. Scanning electron microscopy

Surface topography of the different resins were examined by SEM; as shown in Fig. 5, PAmSnSb surface structure is different from both PAmSnSi and PAmSnSiSb. Larger agglomeration of particles was shown in PAmSnSb, with homogeneous and controlled surface flakes. However, intra- and/or interconnected pore system were observed in PAmSnSi and PAmSnSiSb. Mesoporous slit-like and cylindrical pore shapes characterize this system. As indicated by the average pore radius obtained using BJH procedure, the degree of meso- and micro-porosity in PAmSnSi < PAmSnSb < PAmSnSiSb, which participate in the total surface area of the individual resins.

3.6. Fourier transform-infra red analysis [32]

The help of the FTIR spectra shown in Figs. 6–9 could track the reaction course between the precursors used for preparation of the different resins. Three types of polyacrylamide monomers, namely acrylamide, acrylamide low carboxy content (Am-LCC), and acrylamide high carboxy content (Am-HCC) were used; the differences between their spectra are shown in Fig. 6. A medium peak was observed at about 3,395 cm^{-1}, which is attributed to the stretching –NH mode of normal acrylamide. The same peaks were observed for low carboxylic and high carboxylic

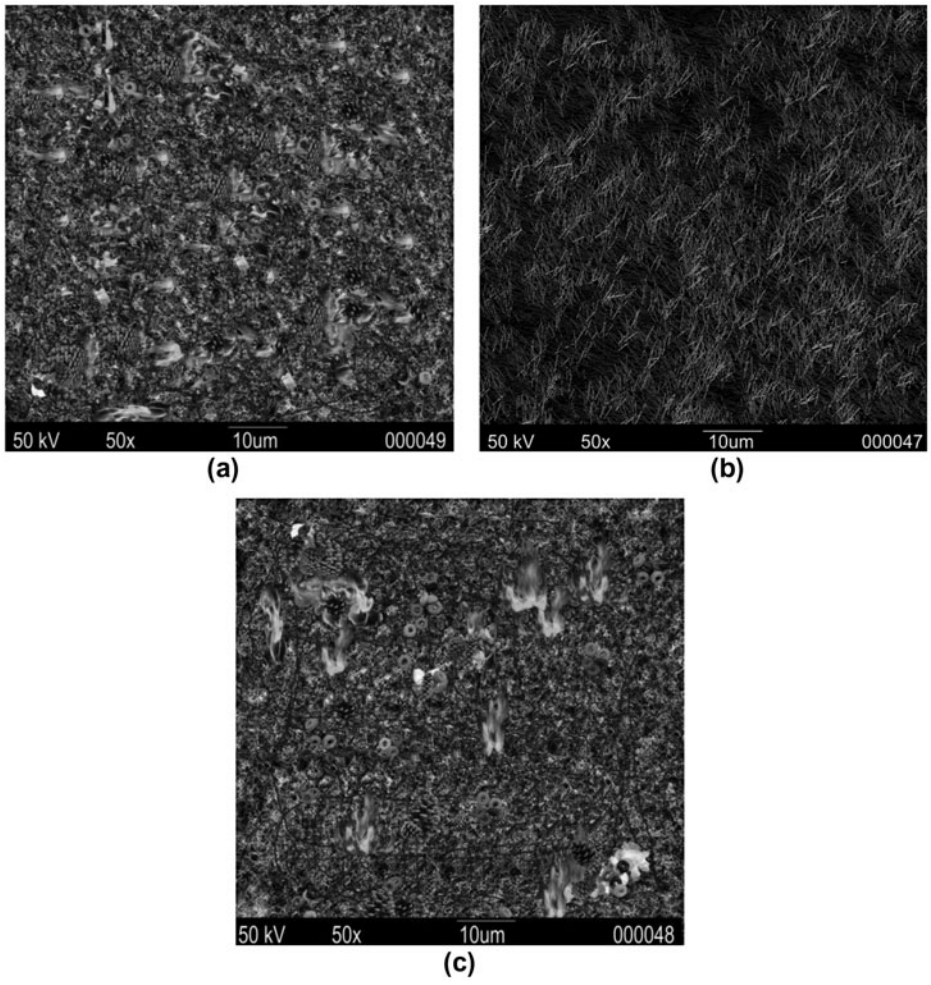

Fig. 5. SEM of PAmSnSi (a), PAmSnSb (b), and PAmSnSiSb (c).

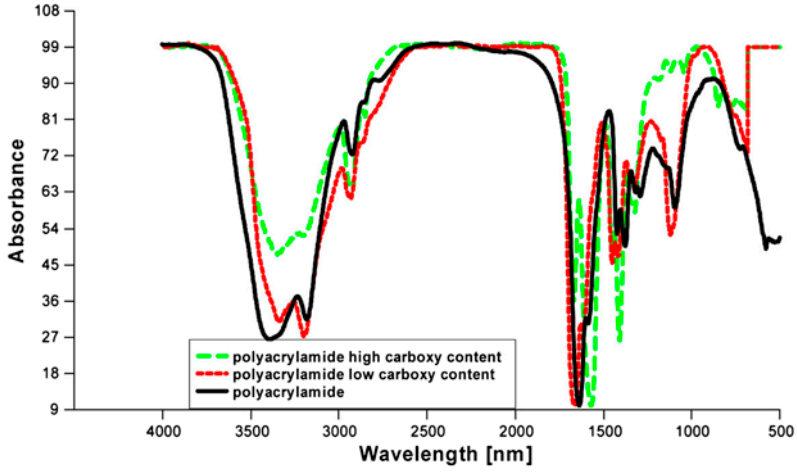

Fig. 6. FTIR Spectra of different polyacrlamide resins.

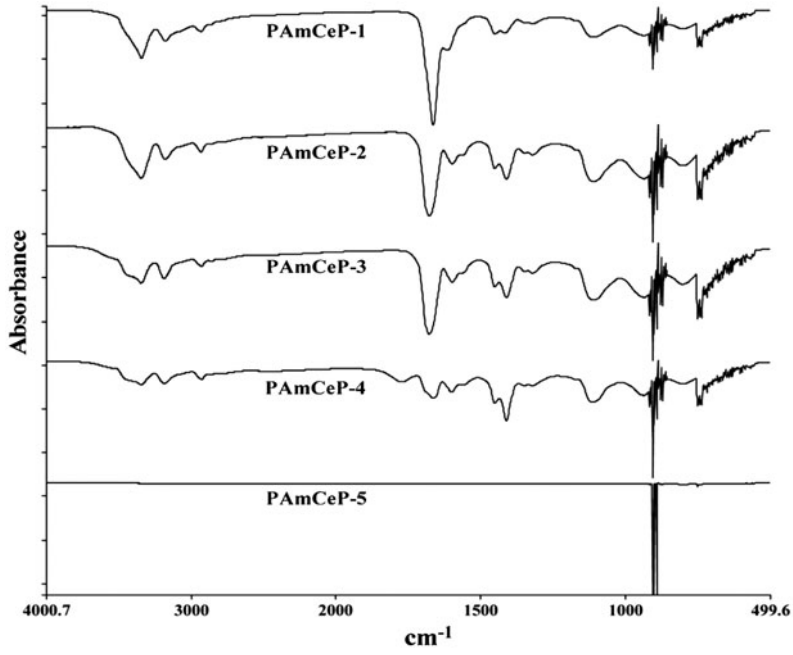

Fig. 7. FTIR Spectra of PAmSnSiSb, thermally treated at different reaction temperatures.

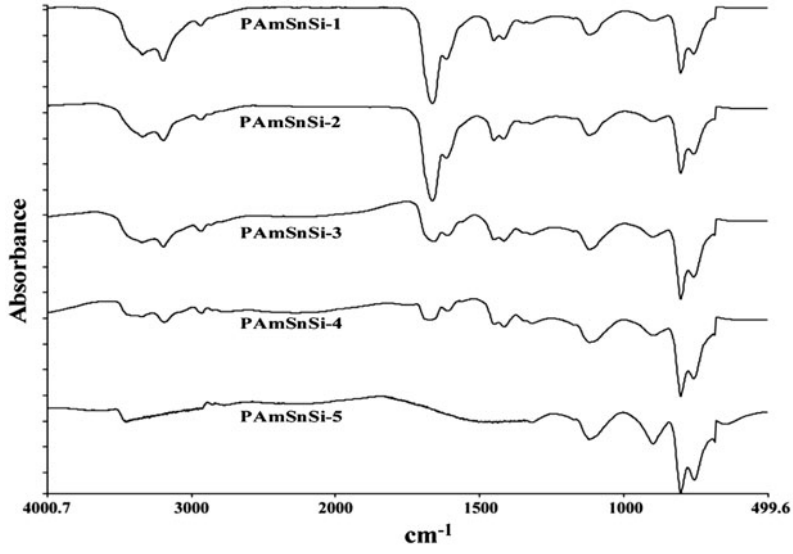

Fig. 8. FTIR Spectra of PAmSnSi, thermally treated at different reaction temperatures.

content acrylamide; the peak became sharper in LCC. However, HCC acrylamide was used during most of the preparation schemes. At 2,929 cm^{-1}, a medium peak was shown, which could be attributed to the aliphatic –CH. The bending mode of $–NH_2$ was observed at about 1,577 cm^{-1}, while the stretching mode of carbonyl and C–N group was observed at about 1,695 and 1,430 cm^{-1}. Figs. 7–9 show the effect of thermal treatment on the active groups of the PAmSnSiSb, PAmSnSi, and PAmSnSb, at 50, 100, 200, 400, and 600 ℃, labeled with 1–5, respectively. During the reaction course, the C=O group was consumed. This could be elucidated by the disappearance of the corresponding peak at about 1,695 cm^{-1} and appearance of some

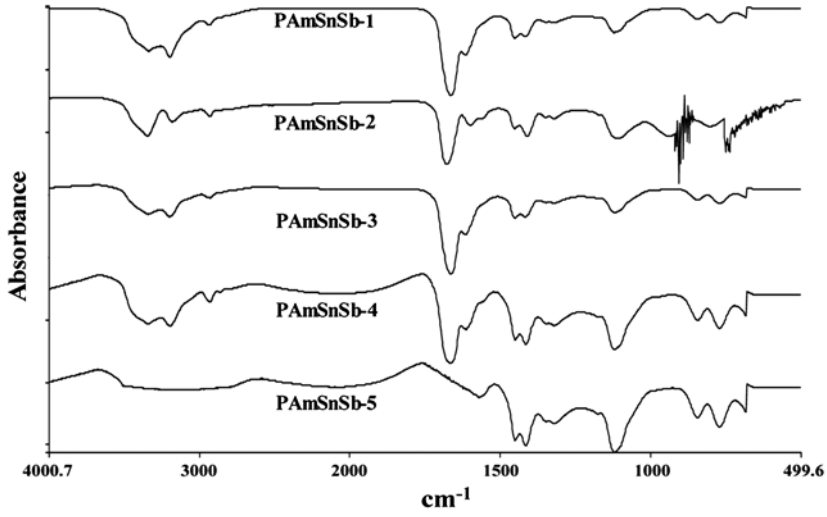

Fig. 9. FTIR Spectra of PAmSnSb, thermally treated at different reaction temperatures.

peaks at about 1,050–110 cm^{-1} which is attributed to conversion of C=O to C–O in the new resin skeleton [17–22].

As shown in Fig. 7, a strong and broad band around 3,400 cm^{-1} is found, which can be ascribed to –OH stretching frequency, and hence shows the presence of lattice water in PAmSnSi. Another peak with a maximum at 1,630 cm^{-1} can be attributed to H–O–H bending, which represents the strongly bonded –OH groups in the matrix [17]. An assembly of broad peaks in the region 650–800 cm^{-1} may be due to the presence of aqua waging, twisting, and rocking modes of metal oxygen bond. Absorption in the range about 1,450–1,600 cm^{-1} referred to stretching of C–N bonds [21]. The peak at 3,200 cm^{-1} may be attributed to be symmetric stretching vibration of the NH_2 group, band at 2,900 cm^{-1} related to C–H group. The spectrum showed a strong band at 1,100 cm^{-1}, which indicates the presence of silicate. It was noticed also an absorption band at 1,673 cm^{-1}, which characteristic to $–CONH_2$ of PAm [22].

The FTIR spectrum of hybrid cation-exchange material PAmSnSb is represented in Fig. 8, which revealed the presence of the superficial water molecules in addition to the metal oxygen, M- OH stretching band. A broad band to the region 3,350 cm^{-1} may be due to the presence of surface water molecules in addition to–OH group. The peak at 3,200 cm^{-1} may be attributed to be symmetric stretching vibration of the NH_2 group. The peak at 1,600 cm^{-1} may be due to the interstitial water present in the composite material [19,20]. An assembly of three peaks in the 500–800 cm^{-1} region showed the self-assurance of M- oxygen bonds present within the material. The additional band at 1,400 cm^{-1} can be ascribed to stretching vibration of C–N; this indicates that the material contains a considerable amount of polyacrylamide. The peak at 1,223 cm^{-1} is characteristic of (NH_2) [22]. The peak at 2,900 cm^{-1} is related to C–H group. Furthermore, it was found the peak at 1,673 cm^{-1} which characteristic to $–CONH_2$ of PAM.

The infrared spectrum of polyacrylamide stannic silicoantimonate is shown in Fig. 9. Nearly, the same absorption bands found across the spectrum of polyacrylamide stannic silicoantimonate were observed in PAmSnSi and PAmSnSb.

With rising the reaction temperature from room temperature, the physically adsorbed water as well as the crystalline water is squeezed out from the exchanger. This could be seen by the gradual decrease in the peaks intensities associated with water molecules at about 3,200–3,400 cm^{-1}. Furthermore, these data are in agreement with that obtained from the DTA-TGA measurements. At about, 600°C, the peaks almost diminished because of destruction of the resin skeleton.

3.7. Distribution studies

The distribution coefficients, K_ds, of $^{134}Cs^{+}$, $^{60}Co^{2+}$, $^{90}Sr^{2+}$, and Cd^{2+} on PAmSnSi, PAmSnSb, and PAmSnSiSb were determined by batch method to get an idea of partition behavior of the exchanger toward the separation of metal ions of analytical interest.

3.7.1. The effect of pH

The initial pH value of the solution is an important controlling guideline that must be considered in the course of the adsorption process. The pH comprises

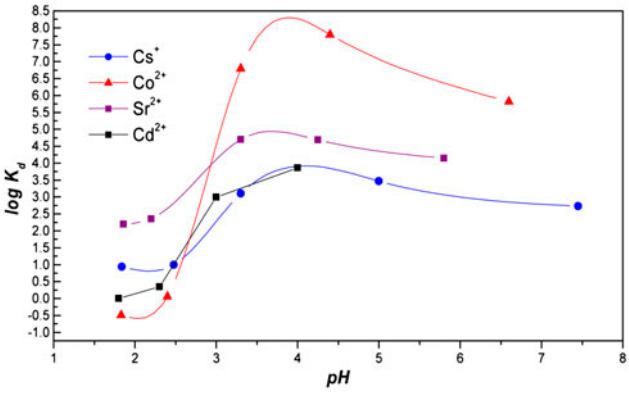

Fig. 10. Effect of pH on the distribution coefficients of Cs^+, Co^{2+}, Sr^{2+}, Cd^{2+}/ PAmSnSi.

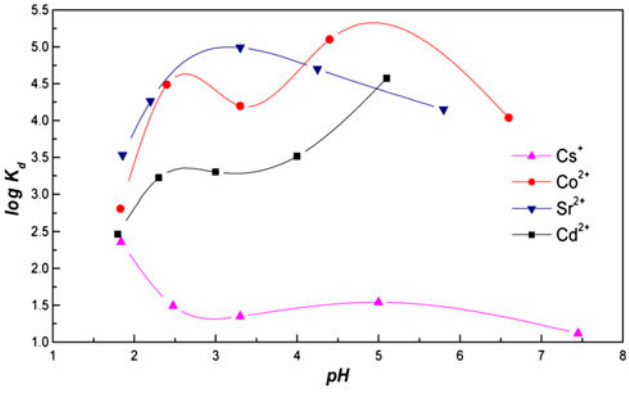

Fig. 11. Effect of pH on the distribution coefficients of Cs^+, Co^{2+}, Sr^{2+}, Cd^2/ PAmSnSb.

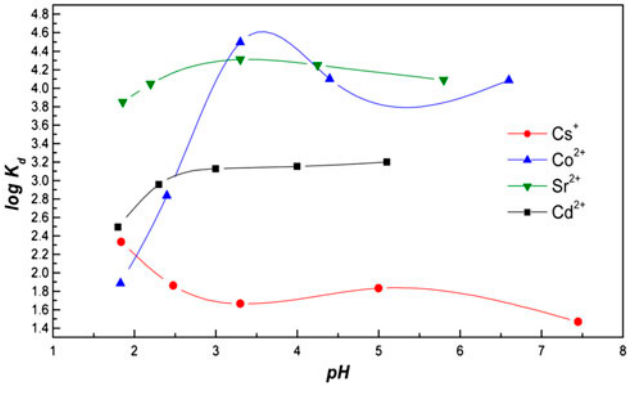

Fig. 12. Effect of pH on the distribution coefficients of Cs^+, Co^{2+}, Sr^{2+}, Cd^2/PAmSnSiSb.

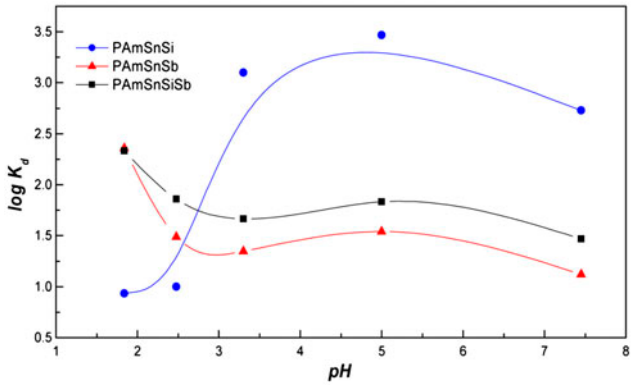

Fig. 13. Effect of pH on the distribution coefficients of Cs^+/(PAmSnSi, PAmSnSb, and PAmSnSiSb).

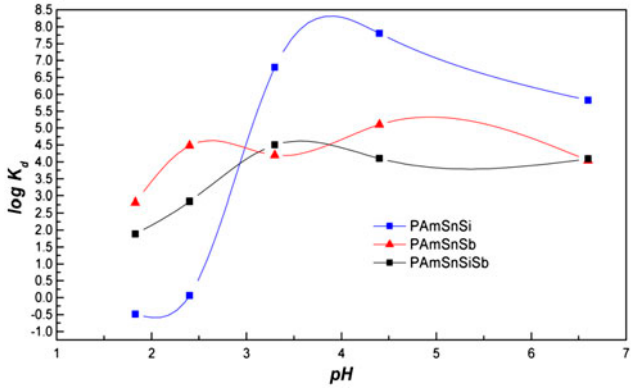

Fig. 14. Effect of pH on the distribution coefficients of Co^{2+}/(PAmSnSi, PAmSnSb, and PAmSnSiSb).

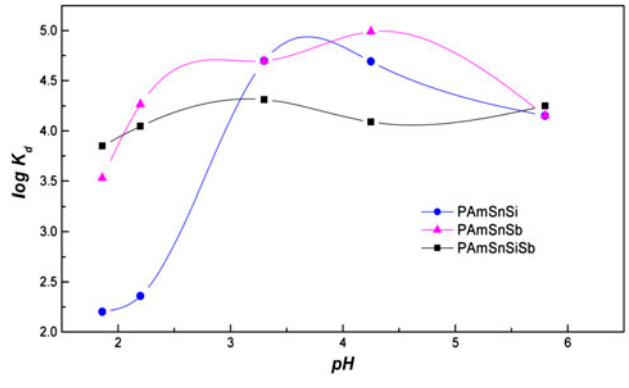

Fig. 15. Effect of pH on the distribution coefficients of Sr^{2+}/(PAmSnSi, PAmSnSb, and PAmSnSiSb).

two kinds of manipulation on metal sorption: an influence upon the solubility and speciation of metal ions in solution, and on the on the whole charge of the sorbent [33]. In order to inquire into the selectivity for the planned metal cations ($^{134}Cs^+$, $^{60}Co^{2+}$, $^{90}Sr^{2+}$, and Cd^{2+}) on the set composites, the distribution coefficients, K_ds were resolved at different pH using constant metal ion concentration, 10^{-3} M, at 30 ± 1°C and after 24 h to reach equilibrium. The K_d results, shown

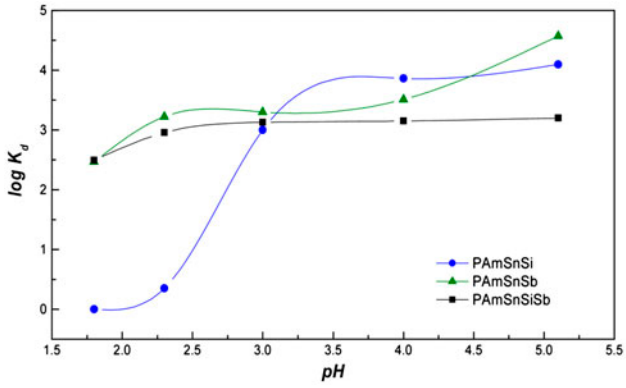

Fig. 16. Effect of pH on the distribution coefficients of Cd^{2+}/(PAmSnSi, PAmSnSb, and PAmSnSiSb).

in Figs. 10–16 for PAmSnSi, PAmSnSb and polyacrylamide stannic silicoantimonate explain that the cation's sorption on the prepared hybrids is restrained by aqueous phase pH. As the pH increase, the distribution coefficient of the cation's increases. Sorption hits a maximum at a pH of 4.0–0.5.

The reason for low sorption in acidic solution is the competition between the excess of H^+ ions into the medium and positively charged cationic species present in the solution [33]. Furthermore, stronger acid concentrations suppress hydrolysis of the metal ions. Additionally as pH increases, the positive surface charge decreases those results in lower coulomb repulsion of the sorbing metal ions [34]. This trend in pH dependence suggests that the removal of metal ions is favored by a slightly high pH asset value. Therefore, for all the other sorption experiments, ideal pH is taken as 4.0. After this pH mark, by increase pH values the distribution coefficient of the cations decreases, and this due to amphoteric character of the prepared ion exchanger [35]. Equally important, PAmSnSi, PAmSnSb, and PAmSnSiSb composites ion exchanger has an isoelectric point, at 5.75, 6.63, and 5.92, respectively, below which; the surface is positively charged, whereas beyond this point, it is negatively charged. At lower pH values where little adsorption occurs; there is an isoelectric repulsion between cations and positively charged surface of the oxide. As the pH increases, the surface becomes less and less positively charged, and thus, the repulsion between cations and the sorbent surface will decrease. In the present study, the linear relations between log k_d and pH not observed, which prove the nonideality of the exchange reaction. The nonideality may due to a different mechanism such as physical adsorption, chemical reaction or other effects, which takes place besides the ion-exchange process [36]. It was found that, the selectivity order of the investigated $^{134}Cs^+$, $^{60}Co^{2+}$, $^{90}Sr^{2+}$, and Cd^{2+} on PAmSnSi, PAmSnSb, and PAmSnSiSb at the same conditions has the following sequence:

$$Co^{2+} > Sr^{2+} > Cd^{2+} > Cs^{+}$$

This sequence is in accordance with the dehydrated radii of the exchanging ions [36]. Ions with the smaller anhydrated radii easily go in the pores of the exchanger, which results in stronger adsorption. The attraction between cations and anions in ionic crystals obey Coulomb's law on the demands for ions of equal charge; a small ion either will be attracted to a greater force or held more tightly than a larger ion.

Figs. 13–16 show the effect of pH on k_d of the individual cation on the different prepared composite's ion exchanger. The K_d of $^{134}Cs^+$/PAmSnSi has higher value than that on PAmSnSb and PAmSnSiSb. Moreover, the k_d reached a maximum value at certain pH, after which, the k_d decrease. These results indicate that PAmSnSi, PAmSnSb, and PAmSnSiSb have zero point charge, ZPC values less than that obtained by titration methods [37]. The k_d of $^{60}Co^{2+}$, $^{90}Sr^{2+}$, and Cd^{2+} on PAmSnSi, PAmSnSb, and PAmSnSiSb have the following order:

$$K_d^{Co^{2+}}/\text{PAmSnSi} > \text{PAmSnSb} > \text{PAmSnSiSb}$$
$$K_d^{Sr^{2+}}/\text{PAmSnSb} > \text{PAmSnSi} > \text{PAmSnSiSb}$$
$$K_d^{Cd^{2+}}/\text{PAmSnSi} > \text{PAmSnSb} > \text{PAmSnSiSb}$$

3.7.2. Effect of concentration

The effect of metal ion concentration during the sorption process has been studied at pH 4.0, equilibration time of 24 h, and 0.0001–0.05 M metal ion concentration over the temperature range of 30–60 °C, as shown in Figs. 17–28. The k_d markedly decrease with

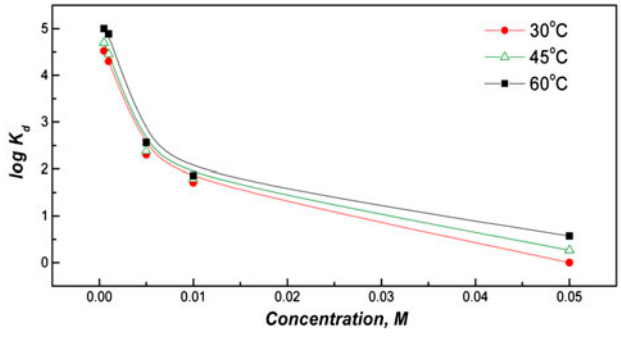

Fig. 17. Distribution coefficient of Cs^+/PAmSnSi at different concentrations and different reaction temperatures at pH 4.

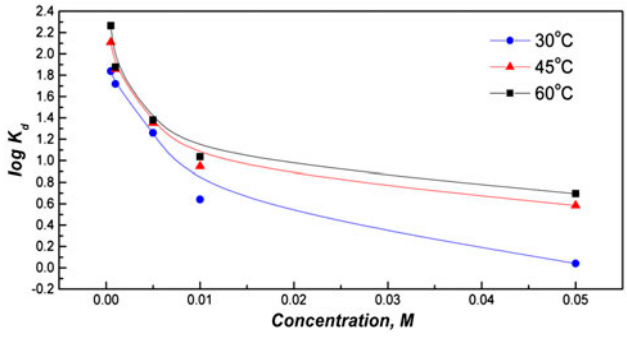

Fig. 18. Distribution coefficients of Cs^+/PAmSnSb at different concentrations and different reaction temperatures at pH 4.

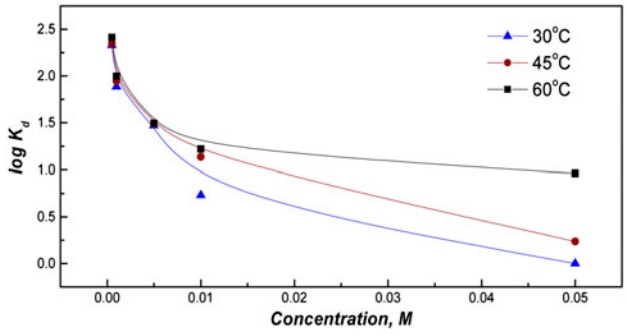

Fig. 19. Distribution coefficients of Cs^+/PAmSnSiSb at different concentrations and different reaction temperatures at pH 4.

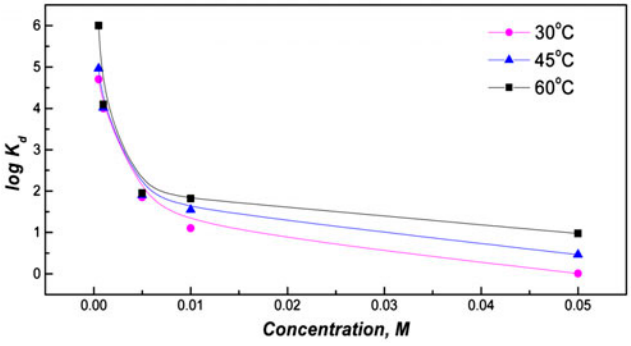

Fig. 20. Distribution coefficients of Co^{2+}/PAmSnSi at different concentrations and different reaction temperatures at pH 4.

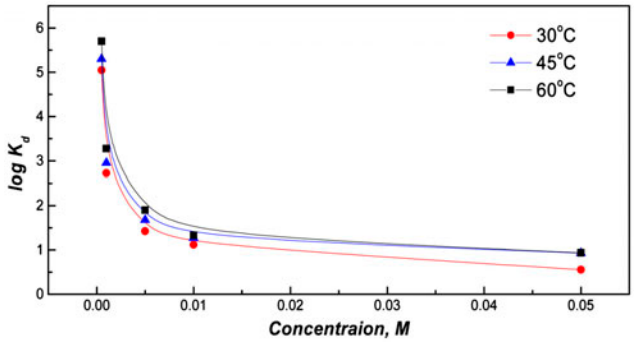

Fig. 21. Distribution coefficients of Co^{2+}/PAmSnSb at different concentrations and different reaction temperatures at pH 4.

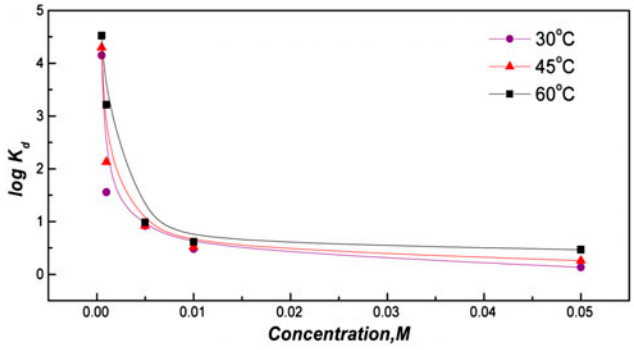

Fig. 22. Distribution coefficients of Co^{2+}/PAmSnSiSb at different concentrations and different reaction temperatures at pH 4.

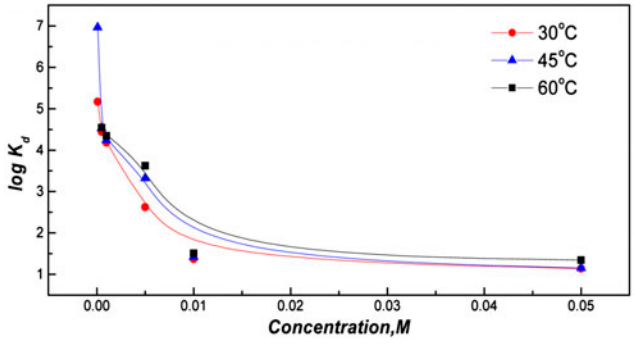

Fig. 23. Distribution coefficient of Sr^{2+}/PAmSnSi at different concentrations and different reaction temperatures at pH 4.

increasing the metal ion concentration. This may be due to increase in the repulsive forces between the same charged species with the increase in the metal ion concentration. Thus, this will hinder the mobility of metal ion toward the exchangeable sites [33]. In addition to besides these figures, it demonstrate the effect of temperature on the k_d for the ion exchange of metal ions onto prepared composites.

The effect of temperature throughout the sorption process is important because not only it affects the rate and extent of sorption, but also since temperature dependence of sorption provides information about possible sorbate–sorbent interaction [38]. In the temperature range of 30–60°C, the k_d of the set composite ion exchangers for Cs^+, Co^{2+}, Sr^{2+}, and Cd^{2+} ions were

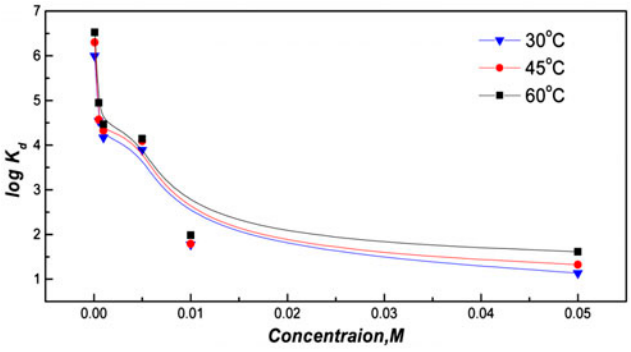

Fig. 24. Distribution coefficient of Sr^{2+}/PAmSnSb at different concentrations and different reaction temperatures at pH 4.

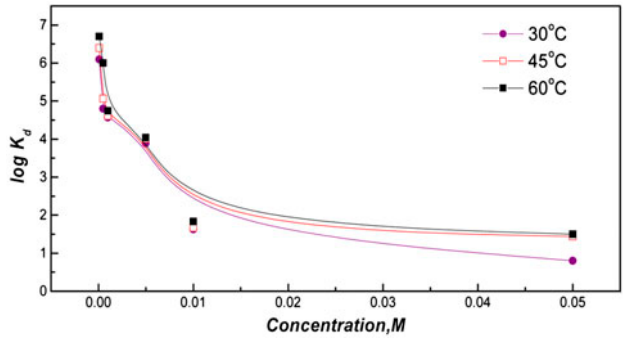

Fig. 25. Distribution coefficient of Sr^{2+}/PAmSnSiSb at different concentrations and different reaction temperatures at pH 4.

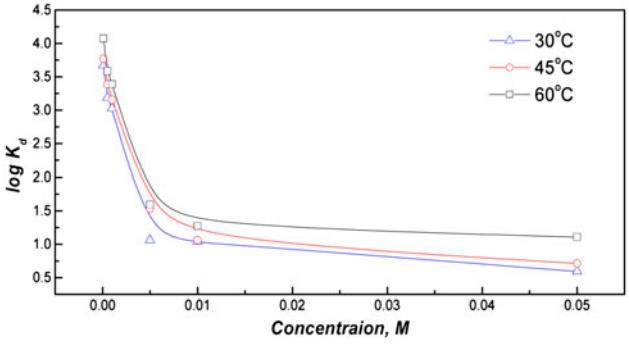

Fig. 26. Distribution coefficient of Cd^{2+}/PAmSnSi at different concentrations and different reaction temperatures at pH 4.

determined. It can be seen that temperature has only one important effect on the ion exchange Cs^+, Co^{2+}, Sr^{2+}, and Cd^{2+} ion's removal using any type of the prepared composite's ion exchanger, thus an increase in k_d of the metal ions with a rise in temperature was observed. It may be observed that higher temperatures motivate the metal ions for enhancing sorption at the coordinating sites of the minerals. In addition, the cations move faster when temperature increases. From the potential point of view, specific or electrostatic interactions become weaker and the ions become smaller, since solvation is reduced [39]. It was evident from the previous equilibrium sorption studies for temperature effect that temperature elevation improves ion sorption for all studied sorption processes [40], which gives prediction that the studied ion-exchange processes were endothermic processes for all studied composites ion exchangers [38]. It can be seen from these figures that the distribution coefficients of $^{134}Cs^+$, $^{60}Co^{2+}$, $^{90}Sr^{2+}$, and Cd^{2+} on PAmSnSi, PAmSnSb, and PAmSnSiSb have the following order:

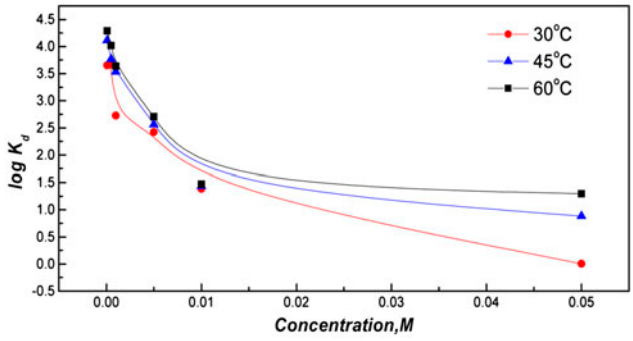

Fig. 27. Distribution coefficient of Cd^{2+}/PAmSnSb at different concentrations and different reaction temperatures at pH 4.

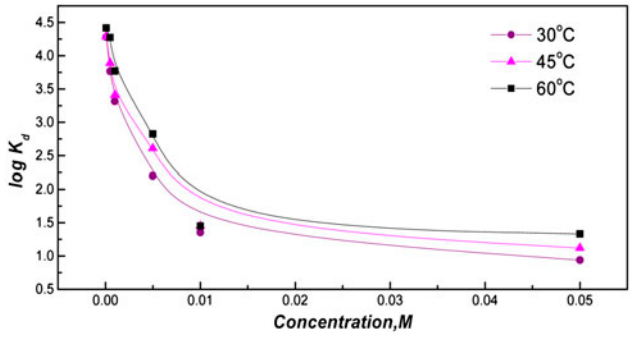

Fig. 28. Distribution coefficient of Cd^{2+}/PAmSnSiSb at different concentrations and different reaction temperatures at pH 4.

$K_d^{Cs^+}$/PAmSnSi > PAmSnSiSb > PAmSnSb
$K_d^{Co^{2+}}$/PAmSnSb > PAmSnSi > PAmSnSiSb
$K_d^{Sr^{2+}}$/PAmSnSiSb > PAmSnSb > PAmSnSi
$K_d^{Cd^{2+}}$/PAmSnSiSb > PAmSnSb > PAmSnSi

Because of distribution coefficient determination, the separation factor is considered as the relative predisposition of two ions to be adsorbed on exchanger from solutions of equal concentration. It could be expressed through the ratio of the distribution coefficients of the elements to be separated as follows:

$$\alpha_B^A = \frac{k_d^A}{k_d^B} \tag{3}$$

where k_d^A and k_d^B are the distribution coefficients for the two competing species A and B in the ion-exchange system.

In order to demonstrate the separation capability of these different composite ion exchangers, separation factors of $^{134}Cs^+$, $^{60}Co^{2+}$, $^{90}Sr^{2+}$, and Cd^{2+} ions pairs at selected pH were calculated. At pH 1.8, the binary separations predicted of α_{Cs}^{Sr}, α_{Cd}^{Sr} and α_{Co}^{Sr} were 18.473, 158.5, and 490.7, at pH 3.3, α_{Cs}^{Co}, α_{Sr}^{Co} and α_{Cd}^{Co} were 4963.7, 125.25, and 6277.7 on PAmSnSi, respectively. On the other hand, on PAmSnSb at pH 1.84, α_{Cs}^{Sr}, α_{Cd}^{Sr} and α_{Co}^{Sr} were 14.86, 11.67, and 5.297, at pH5, α_{Cs}^{Co}, $\alpha_{Sr}^{Co}$and α_{Cd}^{Co} were 3647.9, 2.5 and 38.9. The separation factors of, α_{Cs}^{Sr}, α_{Cd}^{Sr} and α_{Co}^{Sr} on PAmSnSiSb at pH 2.4 were 153.5, 16.25, and 12.38, at pH 3.3, α_{Cs}^{Co}, α_{Sr}^{Co}, and α_{Cd}^{Co} were 6,807, 15.43, and 235.67, respectively.

As a comparison with other ion-exchange composites, some analytically important binary separations of metal ions viz. Al^{3+}–Hg^{2+}, Cu^{2+}–Hg^{2+}, Cu^{2+}–Th^{4+}, Zn^{2+}–Hg^{2+}, Bi^{3+}–Hg^{2+}, Cd^{2+}–Pb^{2+} were achieved on poly-o-toluidine stannic molybdate columns. Hg^{2+} and Pb^{2+} ions were also selectively separated from synthetic mixtures of metal ions [41]. Several binary separations of metal ions viz. Cd^{2+}–Pb^{2+}, Cd^{2+}–Cu^{2+}, Al^{3+}–Pb^{2+}, Al^{3+}–Cu^{2+}, Zn^{2+}–Pb^{2+}, Zn^{2+}–Cu^{2+} was achieved quantitatively on acrylamide stannic silicomolybdate columns. Pb^{2+} and Cu^{2+} were selectively removed from synthetic mixtures containing Cu^{2+}, Mg^{2+}, Cd^{2+}, Hg^{2+}, Zn^{2+}, and Ba^{2+} and Pb^{2+}, Hg^{2+}, Cd^{2+}, Ba^{2+}, Mg^{2+}, and Ba^{2+}, respectively [42]. In case of cesium separation, it was found that the electrochemically switched adsorption process of Cs^+ by nickel hexacyanoferrate on porous three-dimensional carbon felt, NiHCF/PTCF electrodes proceeded in two main steps, that is, an electrically switched ion exchange, ESIX step with a fast adsorption rate and an ion diffusion step with a slow diffusion rate. Meanwhile, the NiHCF/PTCF film electrode showed adsorption selectivity for Cs^+ in preference to Na^+ [43,44].

4. Conclusion

PAmSnSi, PAmSnSb and polyacrylamide stannic silicoantimonate hybrid exchangers were prepared and characterized using different tools. They proved they are amorphous in nature, except for polyacrylamide stannic silicoantimonate was semicrystalline. They were chemically, thermally stable and possess improved selectivity toward $^{134}Cs^+$, $^{60}Co^{2+}$, $^{90}Sr^{2+}$, and Cd^{2+} ions. They are promising and useful materials, where an effective method is needed for the removal and isolation of hazardous ions from radioactive or industrial effluents

References

[1] J. Song, Z. Luo, D.K. Britt, H. Furukawa, O.M. Yaghi, K.I. Hardcastle, C.L. Hill, A multiunit catalyst with synergistic stability and reactivity: A polyoxometalate-metal organic framework for aerobic decontamination, J. Am. Chem. Soc. 133 (2011) 16839–16846.
[2] D. Britt, D. Tranchemontagne, O.M. Yaghi, Metal-organic frameworks with high capacity and selectivity for harmful gases, Proc. Nat. Acad. Sci. USA 105 (2008) 11623–11627.
[3] A. Khan, A.M. Asiri, M. Abdul Rub, N. Azum, A.A.P. Khan, S.B. Khan, M.M. Rahman, I. Khan, Synthesis, characterization of silver nanoparticle embedded polyaniline tungstophosphate-nanocomposite cation exchanger and its application for heavy metal selective membrane, Composites Part B: Eng. 45 (1) (2013) 1486–1492.
[4] Q. Yuan, N. Li, Y. Chi, W. Geng, W. Yan, Y. Zhao, X. Li, B. Dong, Effect of large pore size of multifunctional mesoporous microsphere on removal of heavy metal ions, J. Hazard. Mater. 254–255(15) (2013) 157–165.
[5] D. Ding, Y. Zhao, S. Yang, W. Shi, Z. Zhang, Z. Lei, Y. Yang, Adsorption of cesium from aqueous solution using agricultural residue—Walnut shell: Equilibrium, kinetic and thermodynamic modeling studies, Water Res. 47(7) (2013) 2563–2571.
[6] D.R. Raut, P.K. Mohapatra, M.K. Choudhary, S.K. Nayak, Evaluation of two calix-crown-6 ligands for the recovery of radio cesium from nuclear waste solutions: Solvent extraction and liquid membrane studies, J. Membr. Sci. 429 (2013) 197–205.
[7] K. Lv, L.P. Xiong, Y.M. Luo, Ion exchange properties of cesium ion sieve based on zirconium molybdopyrophosphate, Colloids Surf. A 433(20) (2013) 37–46.
[8] G.M. Ibrahim, B. El-Gammal, I.M. El-Naggar, Selectivity modification of sodium and cesium ions on silicon antimonate, Curr. Top. Colloid Interface Sci. 6 (2003) 159–163.
[9] S.A. Shady, B. El-Gammal, Diffusion pathways of sodium and cesium ions in the particles of titanium(IV) antimonate, Colloids Surf. A 268 (2005) 7–11.
[10] B. El-Gammal, S.A. Shady, Chromatographic separation of sodium, cobalt and europium on the particles of zirconium molybdate and zirconium silicate ion exchangers, Colloids Surf. A 287 (2006) 132–138.
[11] B. El-Gammal, G.M. Ibrahim, H.H. El-Nahas, Thermodynamic and sorption behavior of U(VI) and Th(IV) on unsaturated polyester–styrene polymeric beads, J. Appl. Polym. Sci. 100 (2006) 4098–4106.
[12] H.H. El-Nahas, F.H. Khalil, G.M. Ibrahim, B. El-Gammal, Preparation of unsaturated polyester-styrene beads using gamma irradiation and chemical polymerization routes for use in the recovery of some alkali metal ions, J. Appl. Polym. Sci. 104(2) (2007) 1149–1160.

[13] E.A. Hegazy, B. El-Gammal, F.H. Khalil, T.M. Mabrouk, Evaluation of anionic- and cationic-supported hydrogel membranes for sorption of Th(IV) and U(VI) Ions from nitric acid medium, J. Appl. Polym. Sci. 102 (2006) 320–332.
[14] G.M. Ibrahim, F.H. Khalil, B. El-Gammal, Interaction of La^{3+} and Ce^{4+} with polyethylene and polypropylene polymeric matrices, J. Appl. Polym. Sci. 103 (2007) 2141–2151.
[15] G.M. Ibrahim, M.I. Ahmad, B. El-Gammal, Structural development of TMMA and SSQXN-8 as porous chelating resins, J. Appl. Polym. Sci. 113(5) (2009) 3038–3048.
[16] J. Song, Z. Luo, H. Zhu, Z. Huang, T. Lian, A.L. Kaledin, D. G. Musaev, S. Lense, K.I. Hardcastle, C.L. Hill, Synthesis, structure, and characterization of two polyoxometalate photosensitizer hybrid materials, Inorg. Chim. Acta 363 (2010) 4381–4386.
[17] B. El-Gammal, G.M. Ibrahim, K.F. Allan, I.M. El-Naggar, Modeling the PAAc-AN-TV surface using ^{134}Cs and $^{152+154}Eu$ sorption, J. Appl. Polym. Sci. 113(5) (2009) 3405–3416.
[18] G.M. Ibrahim, B. El-Gammal, I.M. El-Naggar, Synthesis and characterization of novel materials Tin potassium vanadate and zirconium potassium vanadate inorganic multi-component ion exchangers, Sep. Sci. Technol. 46 (2011) 664–678.
[19] G.M. Ibrahim, M.I. Ahmad, B. El-Gammal, I.M. El-Naggar, Selectivity sequence of multivalent lanthanides for their separation on antimonate based exchangers, Sep. Sci. Technol. 46 (2011) 2549–2565.
[20] B. El-Gammal, K.F. Allan, Ion exchange reversibility of some radionuclides on zirconium tungstosuccinate and zirconium tungstosalicylate at their solid-liquid interfaces, Sep. Sci. Technol. 47 (2012) 131–146.
[21] S.S. Metwally, B. El-Gammal, H.F. Aly, S.A. Abo-El-Enein, Removal and separation of some radionuclides by polyacrylamide based Ce(IV) phosphate from radioactive waste solutions, Sep. Sci. Technol. 46 (2011) 1808–1821.
[22] B. El-Gammal, S.S. Metwally, H.F. Aly, S.A. Abo-El-Enein, Verification of double-shell model for sorption of cesium, cobalt, and europium ions on polyacrylonitrile-based Ce(IV) phosphate from aqueous solutions, Desalin. Water Treat. 46 (2012) 124–138.
[23] E.A. Abdel-Galil, Chemical studies and sorption behavior of some hazardous metal ions on polyacrylamide stannic (IV) molybdophosphate as 'organic—inorganic' composite cation—exchanger, PhD Thesis Ain Shams University, Cairo, 2011.
[24] A.A. Khan, Inamuddin, M.M. Alam, Preparation, characterization and analytical applications of a new and novel electrically conducting fibrous type polymeric–inorganic composite material: Polypyrrole Th(IV) phosphate used as a cation-exchanger and Pb(II) ion-selective membrane electrode, Mater. Res. Bull. 40(2) (2005) 289–305.
[25] X. Gu, F. Chen, B. Zhao, J. Zhang, Photocatalytic reactivity of Ce-intercalated layered titanate prepared with a hybrid method based on ion-exchange and thermal treatment, Superlattices Microstruct. 50(2) (2001) 107–118.
[26] I.M. El-Naggar, G.M. Ibrahim, E.A. El-Kady, E.A. Hegazy, Sorption mechanism of Cs^{+}, $Co2^{+}$ and $Eu3^{+}$ ions onto EGIB sorbent, Desalination 237(1–3) (2009) 147–154.
[27] A.A. Khan, M.M. Alam, New and novel organic–inorganic type crystalline 'polypyrrolel/polyantimonic acid' composite system: Preparation, characterization and analytical applications as a cation-exchange material and Hg(II) ion-selective membrane electrode, Anal. Chim. Acta 504(2) (2004) 253–264.
[28] J. B. Condon, Surface Area and Porosity Determinations by Physisorption Measurements and Theory, in: J. B. Condon (Ed.), Elsevier, Amsterdam, Netherlands, 2006.
[29] T. Khalil, F. Abou El-Nour, B. El-Gammal, A.R. Boccaccini, Determination of surface area and porosity of sol–gel derived ceramic powders in the system TiO_2–SiO_2–Al_2O_3, Powder Technol. 114 (2001) 106–111.
[30] A. Neimark, K.S.W. Sing, M. Thommes, Surface Area and Porosity, in: Ertl, Koezinger, Schueth, Weitkamp (Eds.), Handbook of Heterogeneous Catalysis, 2nd ed., Wiley-VCH verlag GmbH, Berlin, 2008, pp. 721–737.
[31] F.B. Sillars, S.I. Fletcher, M. Mirzaeian, P.J. Hall, Effect of activated carbon xerogel pore size on the capacitance performance of ionic liquid electrolytes, Energy Environ. Sci. 4 (2011) 695–706.
[32] K. Nakamoto, Infrared and Raman Spectra of Inorganic and Coordination Compounds, 6th ed., John Wiley and Sons, New Jersey, 2009.
[33] P. Sharma, Neetu Synthesis, characterization and sorption behavior of zirconium(IV) antimonotungstate: An inorganic ion exchanger, Desalination 267 (2011) 277–285.
[34] P. Sharma, R. Tomar, Synthesis and application of an analogue of mesolite for the removal of uranium(VI), thorium (IV), and europium(III) from aqueous waste, Microporous Mesoporous Mater. 116 (2008) 641–652.
[35] A. Nilchi, R. Saberi, M. Moradi, H. Azizpour, R. Zarghami, Adsorption of cesium on copper hexacyanoferrate–PAN composite ion exchanger from aqueous solution, Chem. Eng. J. 172(1) (2011) 572–580.
[36] I.M. El-Naggar, E.S. Zakaria, I.M. Ali, M. Khalil, M.F. El-Shahat, Chemical studies on polyaniline titanotungstate and its uses to reduction cesium from solutions and polluted milk, J. Environ. Radioact. 112 (2012) 108–117.
[37] S.P. Mishra, S.S. Dubey, D. Tiwari, Inorganic particulates in removal of heavy metal toxic ions: IX. Rapid and efficient removal of Hg(II) by hydrous manganese and tin oxides, J. Colloid. Interface Sci. 279(1) (2004) 61–67.
[38] M.M. Abd El-Latif, M.F. Elkady, Equilibrium isotherms for harmful ions sorption using nano zirconium vanadate ion exchanger, Desalination 255(1–3) (2010) 21–43.
[39] V.J. Inglezakis, M.M. Loizidou, H.P. Grigoropoulou, Ion exchange studies on natural and modified zeolites and the concept of exchange site accessibility, J. Colloid. Interface Sci. 275(2) (2004) 570–576.
[40] M.M. Abd El-Latif, M.F. Elkady, Kinetics study and thermodynamic behavior for removing cesium, cobalt and nickel ions from aqueous solution using nano-zirconium vanadate ion exchanger, Desalination 271(1–3) (2011) 41–54.
[41] S.A. Nabi, R. Bushra, M. Naushad, A.M. Khan, Synthesis, characterization and analytical applications of a new composite cation exchange material poly-o-toluidine stannic molybdate for the separation of toxic metal ions, Chem. Eng. J. 165 (2) (2010) 529–536.
[42] A.M. Khan, S.A. Ganai, S.A. Nabi, Synthesis of a crystalline organic–inorganic composite exchanger, acrylamide stannic silicomolybdate: Binary and quantitative separation of metal ions, Colloids Surf. A 337(1–3) (2009) 141–145.
[43] B. Sun, X. Hao, Z. Wang, G. Guan, Z.L. Zhang, Y.B. Li, S.B. Liu, Separation of low concentration of cesium ion from wastewater by electrochemically switched ion exchange method: Experimental adsorption kinetics analysis, J. Hazard. Mater. 233–234 (2012) 177–183.
[44] B. Sun, X. Hao, Z. Wang, Z. Zhang, S. Liu, G. Guan, Continuous separation of cesium based on NiHCF/PTCF electrode by electrochemically switched ion exchange, Chin. J. Chem. Eng. 20(5) (2012) 837–842.